International Journal on Engineering Technology (InJET)

www.kec.edu.np/kec-journal/
Volume 2, issue no. 1, Dec 2024, Page 117-134
Received Date: Aug 04, 2024
Accepted Date: Sept 23, 2024
ISSN: 3021-940X (Print)
DOI: https://doi.org/10.3126/injet.v2i1.72561

Enhancing Electric Bicycle Efficiency: Investigating Regenerative Braking and Pedal Charging Systems

Ram Krishna Mainali[1, *], Kushal Kafle[2], Sagar Bhattarai[3], Rujan Buyo[4], Rupesh Lal Karn[5]

[1]Department of Automobile and Mechanical Engineering, Thapathali Campus, IOE, TU, Kathmandu, Nepal, mainalisanjeet@gmail.com
[2]Department of Automobile and Mechanical Engineering, Thapathali Campus, IOE, TU, Kathmandu, Nepal, thekushalkafle@gmail.com
[3]Department of Automobile and Mechanical Engineering, Thapathali Campus, IOE, TU, Kathmandu, Nepal, sagarbhattarai000@gmail.com
[4] Department of Automobile and Mechanical Engineering, Thapathali Campus, IOE, TU, Kathmandu, Nepal, ru.buyo17@gmail.com
[5]Department of Automobile and Mechanical Engineering, Thapathali Campus, IOE, TU, Kathmandu, Nepal, rupeshkarn@tcioe.edu.np

Abstract

Electric bicycles (e-bikes) are gaining global popularity as part of the broader shift towards electric vehicles (EVs). This research presents a regenerative electric bicycle designed to maximize energy efficiency, aiming for a top speed of 45 km/h and a range of 50 km. The bicycle incorporates two key energy recovery systems: a downhill regenerative system that captures braking energy and converts it into electricity, and a pedal charging system that converts pedaling kinetic energy to recharge the battery. A digital signal processing system seamlessly switches between charging and electric drive based on rider input. This study examines the effectiveness of these systems. The regenerative braking system achieved an impressive 30.9% efficiency in capturing energy during testing. The pedal charging system initially demonstrated an efficiency of 2.98%. MATLAB simulations revealed clear trends in force and power requirements across different grades (0°, 2.5°, 5°, 7.5°, and 10°), highlighting the crucial role of aerodynamic drag and gradient resistance in influencing performance and energy efficiency. While controlled testing environments require further real-world evaluation, these findings underscore the promising potential of regenerative braking and pedal charging for enhancing electric bicycle efficiency. This research paves the way for the development of more efficient and accessible electric bicycles, promoting sustainable transportation solutions through the selection of durable, efficient, and environmentally friendly components.

Keywords: Regenerative Electric Bicycle, Energy Efficiency, Digital Signal Processing, Pedal Charging System.

1. Introduction

Bicycle being the emotion of transportation and needs to be upgraded according to the necessity and availability of technologies. The outset of the research article delves into the imperative need for sustainable transportation solutions in the face of escalating environmental concerns and governmental bans on fuel-powered vehicles. With conventional fuel prices rising, the demand for cleaner and more efficient modes of transportation has never been more pressing. Electric bicycles are taking the world by storm; fueled by concerns about climate change and rising fuel costs, e-bikes are emerging as a sustainable and practical transportation option. Research in China and the US leads the charge in developing cleaner, more efficient e-bikes. E-bikes are becoming a popular choice for both recreation and commuting, promoting healthier lifestyles and cleaner cities (Salmeron-Manzano and Manzano-Agugliaro, 2018). China's e-bike market is massive, but managing the surge in popularity of high-powered bikes is a challenge (Wei et al., 2013). While e-bikes produce less pollution than traditional vehicles, there's room for improvement, especially when

*Corresponding Author

considering battery types and electricity sources (Cherry, Weinert and Xinmiao, 2009) has evolved into an eco-friendly mode of transport amidst increasing pollution. Electric bicycles with motors and batteries offer efficient urban mobility, combating rising fuel costs and environmental concerns (Bansal et al., 2020). Sales are soaring, with China leading the way – from a mere 56,000 units in 1998 to a staggering 21 million a decade later (Pattanayak et al., 2017). The economic, social, and environmental benefits of electric vehicles far outweigh their costs (Kumar Choudhary B, Jadoun and Kumar Choudhary, 2014). Research suggests that e-bikes are displacing car trips significantly, reducing traffic congestion and emissions (Bigazzi and Wong, 2020). E-bikes are the fastest-growing transportation segment globally, outselling even conventional bicycles in many countries (Fishman and Cherry, 2016). Studies in Switzerland show that e-bikes can significantly cut greenhouse gas emissions, especially with targeted policies (Bucher et al., 2019). Moreover, the electric bicycle design incorporates solar energy for power generation, with a motor installed on the rear wheel. Innovative designs like solar-powered e-bikes are being developed in India to harness clean energy and combat pollution (Shashank et al., 2021). The auto industry is focusing on advancements in power electronics to improve efficiency in all EVs, including e-bikes reviews trends, strategies, and necessary power electronics for these developments (Emadi, Lee and Rajashekara, 2008).

Adopting renewable energy and transforming transport modes, Wireless charging technologies like inductive power transfer hold promise for a seamless e-bike experience (Pellitteri et al., 2020). A study explores various approaches to designing e-bikes, covering electrical, mechanical, and system-level aspects (Dimitrov, 2018). Researchers have developed a battery charging circuit that allows cyclists to generate electricity through pedaling to charge their devices (Cabuk, 2022). DC-DC converter topologies for BEVs and PHEVs, focusing on aspects like power output, component count, efficiency, and cost, while also evaluating converter architectures for fast charging stations. It concludes that the Multidevice Interleaved DC-DC Bidirectional Converter is ideal for high-power applications, whereas low-power vehicles benefit from topologies like the Sinusoidal Amplitude Converter and Z-Source DC-DC Converter due to their efficiency and low noise, Studies compare different DC-DC converter topologies for e-bikes, considering factors like power output, efficiency, and cost (Chakraborty et al., 2019) (Sousa, Costa Branco and Dente, 2007).

E-bikes typically take 6-8 hours to charge and offer a range of 35-50 km on a single charge at a speed of 20 km/h (Prathyusha et al., n.d.). The increasing focus on sustainable transportation will likely lead to continued growth in the e-bike market (Kontar, Ahn and Hicks, 2022). Regenerative braking can further improve efficiency and range (Muetze and Tan, 2007). The rise of e-bikes will create new business opportunities, such as specialized repair shops (Ramadhan and Dinata, 2021). A study explores the growing interest in sustainable transportation and proposes a design for a foldable electric bicycle to improve portability and functionality of cycling (Johny et al., 2021). Extending hybrid e-bike battery life by utilizing a supercapacitor to handle peak loads can ultimately extend the lifespan of the main battery (Mohan, Paritosh and Jadhav, 2021). Simple power control system for e-bikes using a permanent magnet DC motor to capture braking energy and prevent battery overload (Somchaiwong and Ponglangka, 2006).

The Regenerative Electric Bicycle REB concept integrates innovative regenerative and pedal charging systems to harness kinetic energy during downhill and pedaling, extending the bike's range and reducing environmental impact. The REB enhances overall efficiency and vehicle dynamics, material selection, load analysis, and model design by capturing energy that would otherwise be wasted during braking and manual pedaling. Research is targeted in improving motor choice and fine-tuning the model. This promotes sustainability and a sense of ownership over energy consumption. Furthermore, the seamless switching between charging and electric drive modes based on rider input ensures a smooth and intuitive riding experience, catering to diverse user needs and preferences. Through experimental validation and simulation analysis, our research aims to demonstrate the robust performance and potential impact of the REB design. By optimizing energy recovery and enhancing system efficiency, Envisioning the REB as a promising solution to urban mobility challenges, contributing to a greener and more sustainable future for transportation.

Despite the growing body of research on electric bicycles (e-bikes) and their role in sustainable transportation, a critical knowledge gap persists in optimizing energy capture during pedaling. Current pedal-assisted

charging systems demonstrate limited efficiency, thus impeding the full potential for extending e-bike range and minimizing dependence on battery power. This research directly addresses this gap by investigating methodologies to maximize energy recovered from pedaling.

2. Material and Methodology:

Material selection focuses on economic feasibility, with aluminum alloy chosen for the chassis and traditional steel for the sprockets. A static loading analysis is performed in SOLIDWORKS to ensure the design's viability, evaluating Von Mises stress and equivalent strain. To analyze the forces and power requirements of the electric bike, specific points where different forces are applied are carefully considered.: Point 1 (battery pack and carrier), Point 2 (rider and motor force), Point 3 (transmission force), and Point 4 (rider grip on handlebars).

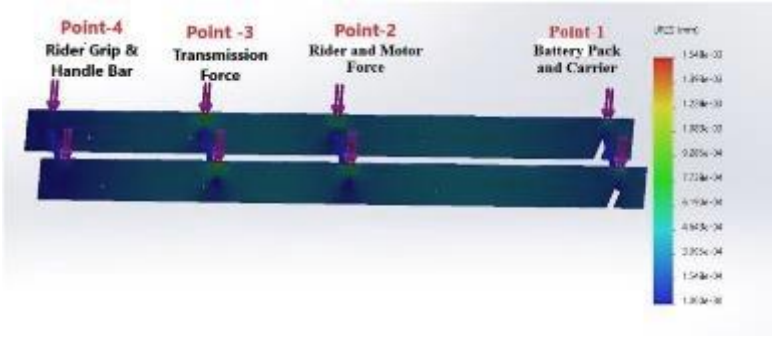

Figure 1. Illustration of force consideration

The points illustrated in Figures 1; i.e. point 1 2, 3, and 4 help visualize the force distribution. By creating a Free Body Diagram (FBD) for each scenario and applying Newton's laws, we derive the equations of motion to understand the forces and moments acting on the bike. This analysis, considering various grade angles (0°, 2°, 5°, 7.5°, and 10°), enables precise calculation of the power requirements. The mode selector, controlled by an Arduino, seamlessly toggles between electric drive and charging modes. Testing confirms the functionality, marking a crucial step toward realizing the innovative design's potential.

2.1. Motor selection:

An aluminum alloy frame offers lightweight strength and easy construction, while standard handlebars and steel sprockets keep costs down. A powerful 800W BLDC motor and lithium-ion battery provide the core performance, with durable steel rims and ply tires ensuring wheel stability. To efficiently charge the 48V battery, a DC-DC boost converter with a minimum input rating of 48V and 18.52A is needed to account for its 90% efficiency and step up the voltage to at least 54V for proper charging.

2.2. Model design of bicycle:

The design is of hybrid electric cycle designed in SOLIDWORKS (2019) software.

2.3. Static Load Analysis:

The static load analysis is conducted using SOLIDWORKS software. Aluminum alloy 6061 is selected for the chassis frame of the electric bicycle due to its high strength, fatigue resistance, hardness, and toughness. The assembly drawing is imported into SOLIDWORKS, along with the dimensions of the chosen material. Simulations are initiated using SOLIDWORKS add-ins, and project studies—such as static, thermal, and strength behavior—are defined. The materials used in the project are assigned, boundary conditions (based on Free Body Diagrams) are applied, and the model is meshed. Afterward, the simulation is executed, and the results are analyzed.

2.3.1. Material Properties

For optimal feasibility, aluminum alloy was chosen as the preferred material for the hybrid electric cycle. The selected alloy exhibits the following key properties: (Yang, Lu and Li, 2013)

Table 1: Property of Alloy Steel

S.N.	Properties	Values
1.	Elastic Modulus	703599.9 kgf/cm²
2.	Poisson Ratio	0.33
3.	Mass Density	0.0027 kg/cm³
4.	Tensile Strength	1265.296956 kgf/cm²
5.	Thermal Conductivity	0.40631 cal/cm.sec.°

2.3.2. Model

The frame of the hybrid electric cycle consists of two aluminum alloy bars with dimensions of 0.96 m in length, 0.7 m in width, and 1 m in thickness. These bars are arranged in a ladder frame design, providing structural support and stability to the vehicle. This configuration ensures a robust and durable framework while maintaining a lightweight and streamlined profile, optimizing both performance and maneuverability.

2.3.3. Meshing

Creating a fine mesh model in SOLIDWORKS is essential for obtaining reliable and accurate simulation results, particularly in complex analyses where detailed resolution is required, thus the fine mesh function of SOLIDWORKS created the following mesh as shown in figure for static analysis preparation.

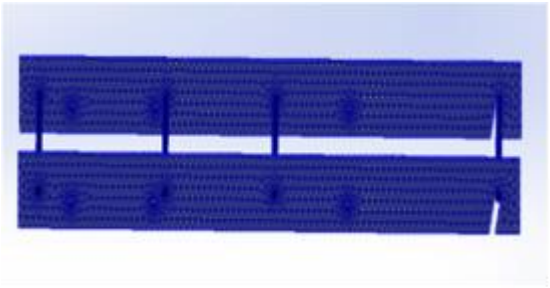

Figure 2. Fine mesh of model

2.4. Working and Design for Hybrid mode

This hybrid electric bike boasts a versatile electric drive system. The 48V battery powers a BLDC motor with a 2:1 gear ratio (14-tooth motor sprocket, 28-tooth wheel sprocket) for efficient propulsion, achieving a wheel speed of 225 rpm at a motor speed of 450 rpm. Downhill rides contribute to battery charge through regenerative braking, with testing showing an open-circuit voltage of 68V captured during downhill simulation. A three-phase rectifier and DC-DC boost converter convert and step up this voltage to 54V for charging the battery. Finally, a manual mode allows for traditional pedaling without generating electricity, focusing solely on rider-powered propulsion.

- ***Mode selector:***

An Arduino microcontroller unit manages switching between electric drive and charging modes based on a throttle voltage signal. When the throttle is at rest (around 0.85V), the charging circuit activates. This circuit uses a full-bridge rectifier with six 2A PN diodes and relays controlled by the Arduino to convert AC current from the motor to DC and send it to a boost converter for charging the battery at 54V. When the throttle is rotated (voltage increases), the Arduino deactivates the charging circuit and activates the electric drive circuit. This drive circuit uses relays to connect the battery directly to the motor controller, enabling electric

propulsion.

2.5. Vehicle dynamics Parameters

1. **Coefficient of Rolling Resistance:**

The coefficient of rolling resistance (C_{rr}) represents the energy lost due to friction between a rolling object and a surface, with lower C_{rr} (around 0.01 for pneumatic tires on pavement) indicating less force needed to maintain constant speed.

2. **Coefficient of drag:**

The coefficient of drag (C_d) is a dimensionless measure denoted as" C_d," representing the resistance of an object to fluid motion, such as air or water. It indicates how much the object decelerates as it moves through the fluid. The C_d depends on factors like the object's shape and size, its speed through the fluid, and properties of the fluid, like density and viscosity. The various parameters required for calculation are noted in the table 2.

Table 2. Parameter Drag Force Calculation

S.N.	Parameters	Value
1.	Coefficient of drag (C_d)	0.5
2.	Coefficient of rolling resistance (C_{rr})	0.004
3.	Frontal area of projection (A_f)	0.7
4.	Density of air at 30 C (ρ)	1.164
5.	Gradient angle (θ) in degree angle	3
6.	Maximum velocity of travel of 2-wheeler in km/h (v)	45
7.	Time for peak-up in seconds (T)	15

3. **Gross Vehicle Weight:**

Gross Vehicle Weight (GVW) simply refers to a vehicle's total weight when fully loaded, encompassing both its own weight (curb weight) and the weight of passengers, cargo, and anything else it carries.

Weights noted for calculation is shown in the table 3.

Table 3. Parameters for Vehicle Weight Calculation

S.N	Parameters	Values (kg)
1.	Curb weight (w_{curb})	10
2.	Motor and controller weight (w_{motor})	3
3.	Battery weight ($w_{battery}$)	5
4.	Rider weight (w_{rider})	75

The calculation for Vehicle Weight (GVW) in Newton is:

$$GVM = \left(w_{curb} + w_{motor} + w_{battery}\right) * 9.81 \quad \text{(Equation 1)}$$
$$= (10 + 3 + 5 + 75) * 9.81$$
$$= 912.33N$$

4. **Rolling Resistance Force**

Rolling resistance force is the resistance encountered by a wheel or tire as it rolls on a surface, caused by tire deformation. Factors affecting this force include tire pressure, size, road condition, load on the tire, and

vehicle speed.

The Formula for Calculating the rolling resistance force

$$F_{rr} = C_{rr} * w \quad \text{(Equation 2)}$$
$$= 0.0004 * 912.33$$
$$= 4.7N$$

5. **Gradient Resistance Force**

Gradient resistance force, also called hill-climbing resistance force, is the force counteracting a vehicle's forward motion when it ascends or descends a slope. This force arises from gravity acting on the vehicle and its load, requiring additional effort to sustain speed or climb uphill.

$$F_{gr} = Vehicle\ weight * \sin(\theta) \quad \text{(Equation 3)}$$
$$= 912.33 * \sin(3)$$
$$= 128.64N$$

6. **Aerodynamic Drag Force**

Aerodynamic drag force, also referred to as air resistance force or drag force, is the force acting in opposition to a vehicle's forward motion as it travels through the air. This resistance force results from collisions between air molecules and the vehicle's surface, necessitating the vehicle's engine or propulsion system to overcome it.

$$(F_{ad}) = \frac{C_d * A * \rho * v^2}{2} \quad \text{(Equation 4)}$$
$$= 63.65N$$

7. **Total Tractive Force:**

The total tractive force represents the net force available to drive a vehicle forward, comprising the sum of all forces acting on the vehicle in the direction of motion. This parameter significantly influences vehicle acceleration, speed, and capability to overcome resistance and ascend hills.

Total Tractive Force (F_{total}) = $F_{rr} + F_{gr} + F_{ad}$ (Equation 5)

$$= 4.7480 + 128.64 + 63.65$$
$$= 197.083N$$

8. **Acceleration Force**

The acceleration required to reach the maximum velocity (V_{max}) of a vehicle within a given time (T) can be calculated by

Acceleration= $\frac{V_{max} - V_0}{T}$ (Equation 6)

Acceleration to reachV_{max} in T second=
3.3333 m/s^2

Force required to pick up: (Equation 7)

$$(F_{acc}) = \frac{w_{gross}}{9.81 * acceleration}$$
$$= \frac{912.33}{9.81 * 3.333}$$
$$= 309.969N$$

9. **Distance covered during acceleration:**

The distance covered by a vehicle during acceleration from rest to a given velocity can be calculated using the following formula:

Distance covered during acceleration:

$$(a_{dist}) = 0.5 * a * T^2 = 0.5 * 3.333 * 15^2 = 374.96m$$ (Equation 8)

10. **Power required during acceleration:**

Power required during acceleration (Peak power):

Power required during acceleration

$$\text{(Peak power):} = \frac{(F_{acc}+F_{rr}+F_{ad})*a_{dist}}{T} = \frac{(309.969 + 4.784 + 63.65) * 374.96}{15} = 945.8166Kw$$ (Equation 9)

11. **Required rotational speed of the motor:**

The rotational speed of a BLDC motor can be calculated using the following formula:

Rotational speed of the motor

$$(RPM_{motor}) = \frac{v*1000}{3600*2*\pi*28*60} = \frac{45 * 1000}{3600 * 2 * \pi * 28 * 60} = 265.39RPM$$ (Equation 10)

12. **Pedal Force:**

The key distinction lies in the electric motor's supplementary assistance, which can significantly alleviate pedal force demands, particularly when conquering challenging terrain or maintaining higher speeds with less effort and desired to obtain 15 km/hr .

Table 4. Parameter for pedal force calculation

S.N	Parameters	Values
1.	Coefficient of rolling resistance, C_{rr}	0.004
2.	Mass of bicycle and rider, m	93 kg
3.	Drag coefficient, C_d	0.5
4.	Frontal area of electric bicycle, A_f	0.72 m2
5.	Density of air, d	1.164 kg/m3
6.	Slope angle, a	12%

Determining the magnitude of pedal force:

Assuming the desired speed is 15 km/h (i.e., 4.167 m/s). The gear ratio of the manual

Rolling Resistance,

$$F_{rr} = C_{rr} * m * g = 0.004 * 93 * 9.81 = 3.649N$$ (Equation 11)

Aerodynamic Drag,

$$F_a = C_d * A_f * d * v^2 = 0.5 * 0.72 * 1.164 * 4.1672 = 7.276N$$ (Equation 12)

Grade Resistance,

$F_g = m * g * \sin(\alpha)$ (Equation 13)

$= 93*9.81*\sin(6.843)$

$= 108.703N$

Total resistance,

$F = F_{rr} + F_a + F_g$

$= 3.649 + 7.276 + 108.703 = 119.628N$ (Equation 14)

Now, the required power is given by,

Required Power $= TotalResis\tan ce * DesiredSpeed$ (Equation 15)

$= 119.628 * 4.167 = 498.5W$

Cadence of the pedal of electric bicycle is 60 RPM.

Pedal Force $= \frac{Required\ Power}{Cadence * Gear\ Ratio}$ (Equation 16)

$= \frac{498.5}{60 * \frac{18}{32}} = 14.77N$

13. **Magnitude of braking force:**

The braking force is given by

Braking force = Coefficient of friction * Area of braking surface * Force applied on the brake lever * (Equation 17)

Mechanical advantage $= 0.64 * 5080 * 10 * 1 = 32514N$ (Equation 18)

Hence, the magnitude of the braking force that can be generated by applying a force of 10 N on the brake lever of a bicycle with a rim brake system, using rubber brake pads and stainless-steel rims, is 32514 N

14. **Stopping Distance:**

The magnitude of the stopping distance:

The initial speed of the bicycle is 45 km/h (i.e., 12.5 m/s). With the coefficient of friction between them is 0.71 (for city roads and tires) and deceleration rate 8 m/s^2, the stopping distance is given by,

Stopping distance$= \frac{(initial\ speed)^2}{2 * Deceleration\ rate * Coefficient\ of\ friction}$ (Equation 19)

$= \frac{(12.5)^2}{2 * 8 * 0.71} = 13.754m$

3. Results and Discussion:

3.1. Model design

Top View

Front View

Side View

Figure 3: Orthographic view of model

The electric bicycle model depicted in Figure 3 is the final fabricated iteration, featuring a ladder frame structure. This selection offers a well-established design known to optimize weight efficiency while maintaining structural integrity. To guarantee the model's ability to endure various loading conditions encountered during operation, simulations were conducted using a comprehensive set of design parameters. This rigorous process validates the model's capacity to withstand real-world use scenarios.

3.2. Simulation metrices:

a. Structural Analysis and Design Validation

The analysis of the electric cycle frame's structural behavior under static loading conditions serves as a testament to its robustness and reliability for its intended use. This evaluation is achieved through the examination of several key metrics:

- **Von Mises Stress:** As illustrated in Figure 7, the von Mises stress values range from 5.835 MPa to higher levels in critical areas like the rotor, rider interface, and transmission zones. These values indicate the frame's capacity to withstand combined normal and shear stresses. Notably, high stress concentrations in these areas pinpoint potential failure zones, guiding targeted design improvements to enhance frame durability.

- **Equivalent strain:** It is another metric used to assess the deformation of a material under load. In this analysis, the equivalent strain values range from zero, indicating no deformation, to a maximum of 7.498 *10^-5, signifying minimal strain experienced by the frame.

- **Resultant Displacement:** Figure 6 depicts the minimal displacement values experienced by the frame under load, with a maximum value of only 1.548 micrometers. This signifies negligible deformation, ensuring the frame maintains its shape and structural integrity during operation. This translates to stable performance and rider safety.

- **Factor of Safety (FOS):** The FOS values, ranging from 9.451 to 3.297 million, as shown in Figure 5, demonstrate a significant margin of safety for the frame even beyond expected loading conditions. This wide range signifies a design with inherent excess strength to handle unexpected stresses or loads, thereby reducing the risk of failure and bolstering overall reliability.

S.N	Components	Minimum Value	Maximum Value
1.	Von Mises Stress	$5.835e^{+06}$ N/m²	-
2.	Equivalent Strain	0	$7.498e^{-5}$
3.	Resultant Displacement	$1.000e^{-30}$ mm	$1.548e^{-03}$ mm
4.	Factor of Safety	$9.451e^{+00}$	$3.297e^{+06}$

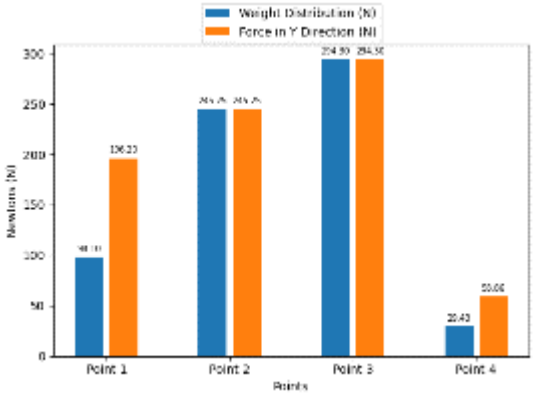

Figure 4. Result of simulation at various point

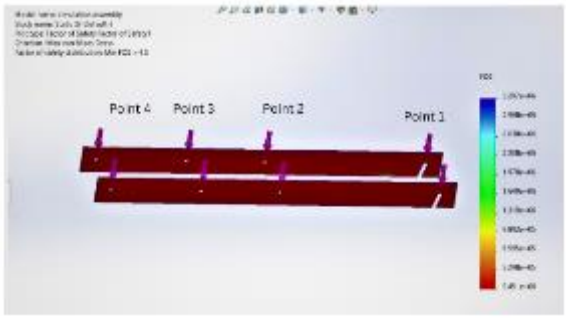

Figure 5. Factor of safety

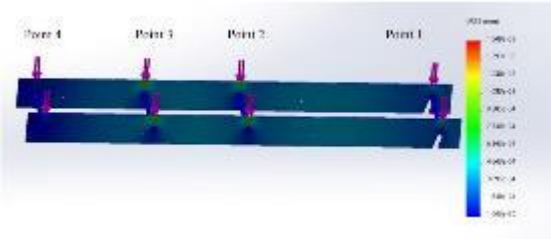

Figure 6. Resultant Displacement

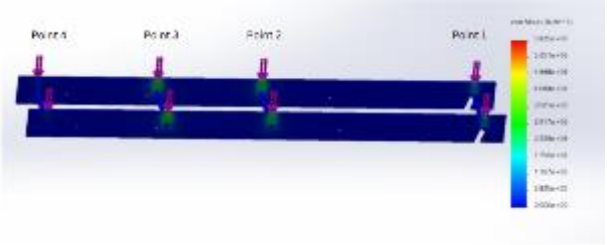

Figure 7. Von Misses stress

In Figure:5 The SOLIDWORKS simulations revealed a range of forces acting on the hybrid electric cycle frame, varying from 98.1 N to 294.3 N. The highest forces were concentrated around the rider, motor, and transmission (245.25 N and 294.3 N) at point 2 and 3 respectively, highlighting these areas as crucial for structural integrity. The analysis also identified the forces exerted by the battery pack and carrier (196.2 N) at point 1 and the rider's grip on the handlebars (58.86 N) at point 4. This comprehensive understanding of force distribution allows for targeted frame optimization, ensuring both performance and durability throughout the lifespan of the hybrid electric cycle. This comprehensive understanding of force distribution allows for targeted frame optimization, ensuring both performance and durability throughout the lifespan of the hybrid electric cycle.

The static analysis conducted using SOLIDWORKS SIMULATION ADD-IN yielded several key results the results are tabulated below in Table-5:

Table 5. Design criteria

S.N	Components	Minimum Value	Maximum Value
1.	Von Mises Stress	$5.835e^{+06}$ N/m²	-
2.	Equivalent Strain	0	$7.498e^{-5}$

3.	Resultant Displacement	$1.000e^{-30}$ mm	$1.548e^{-03}$ mm
4.	Factor of Safety	$9.451e^{+00}$	$3.297e^{+06}$

3.3. E-Mode

Table 6. Output of audrino code

S.N.	Voltage (V)	Relay A1	Relay A2	Relay A3	Relay B1	Relay B2	Relay B3
1.	< 0.85	HIGH	HIGH	HIGH	LOW	LOW	LOW
2.	>= 0.85	LOW	LOW	LOW	HIGH	HIGH	HIGH

The implemented system differentiates between charging and E-drive modes based on the voltage reading from a sensor connected to pin A0. A voltage threshold of 0.85V determines the state of relays controlling the charging circuit and motor. Figure 8 depicts this charging and Figure 9 E-drive mode functionality.

- **Charging Mode:** When the voltage is below 0.85V (likely indicating a low battery), relays A1, A2, and A3 are activated (turned on), engaging the charging circuit. This is signified by a deactivated green light and a stopped motor.
- **E-drive Mode:** Conversely, a voltage reading of 0.85V or higher (potentially indicating sufficient battery level) triggers the activation of relays B1, B2, and B3. This deactivates the charging circuit (green light turns on) and starts the motor, allowing the electric drive system to function using the stored battery charge.

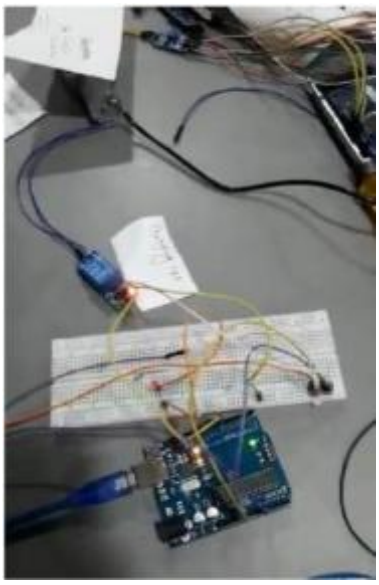

Figure 8. Charging

Figure 9. Drive mode

3.4. Regenerative efficiency:

In the Regenerative Efficiency Test, energy consumption is determined by the difference in wattmeter readings between start and finish points under various conditions.

Regenerative charging efficiency using the provided formula:

Efficiency = (Equation 20)

$$\frac{Energy\ Consumed\ without\ Regenerative\ Braking}{EnergyRegeneratedwithRegenerativeBraking} * 100$$

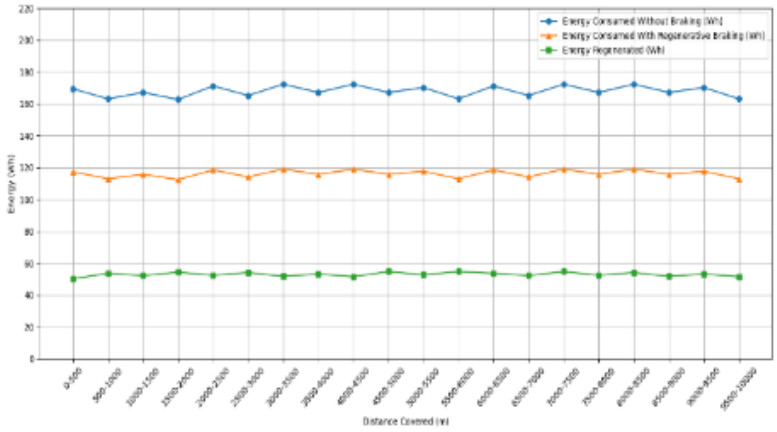

Figure 10. Electric bicycle Regenerative charging Test Data

The reduction in energy consumption and the regeneration of energy during the test of the electric bicycle can be attributed to the efficiency of regenerative braking. Regenerative braking converts the kinetic energy of the bicycle, which would otherwise be lost as heat during braking, back into electrical energy that recharges the battery. On a flat road, braking events are typically fewer and less intense than on hilly terrain, yet the system can still capture significant energy during deceleration phases or minor speed adjustments. In this test, the regenerative braking system effectively captured 792 Wh, reducing the net energy consumption to 1,724 Wh from 2,516 Wh. This efficient energy recovery accounts for the 30.5% combined regenerative percentage, showcasing the effectiveness of the system in harnessing and reusing energy that would otherwise be wasted.

3.5. Pedal charging efficiency:

The efficiency of the pedal charging system was evaluated by comparing the energy generated through pedaling to the energy recaptured by the battery. This was achieved by calculating the change in battery percentage for each test, thereby determining the proportion of energy recaptured relative to that generated by pedaling.

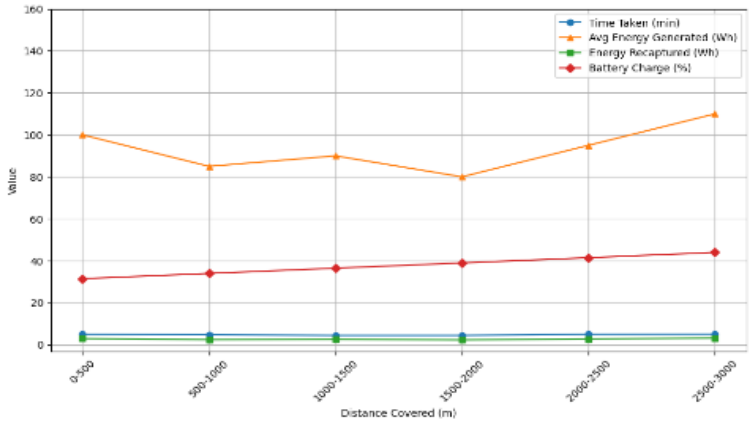

Figure 11. Pedal charging regeneration

Figure11 illustrate the average energy generated, Energy recaptured and battery percentage change within the range of 0-3000 meters at a equal interval 500meters, then those data are utilized for calculating pedal charging efficiency.

To calculate the pedal charging efficiency for the 3 km ride, first calculating

the total energy generated by pedaling and the total energy recaptured to the battery

during the entire ride.

Total Energy Generated by Pedaling = $550Wh$
Total Energy Recaptured to Battery = $2.95 + 2.47 + 2.63 + 2.34 + 2.78 + 3.22 = 16.39Wh$ Equation (21)
Pedal Charging Efficiency = $\frac{Total\ Energy\ Recaptured\ to\ Battery}{Total\ Energy\ Generated\ by\ Pedaling} * 100 = \frac{16.39}{550} * 100$
$= 2.98\%$

The pedal charging system on the electric bicycle demonstrates an average energy generation of 550 Wh over a 3 km ride, with a total energy recapture of 16.39 Wh to the battery, resulting in a pedal charging efficiency of 2.98%. This low efficiency indicates that only a small fraction of the pedaling energy is converted back into electrical energy stored in the battery. Despite this, the battery charge increased from 30% to 42% over the ride, suggesting that the primary contribution to the battery's charge came from the regenerative braking system rather than the pedal charging system. The varying energy recapture at different intervals highlights the efficiency of the regenerative braking in converting kinetic energy back to stored electrical energy, complementing the pedal charging and contributing to the overall increase in battery charge.

3.6. Vehicle dynamics

At various grading condition of 0° grade, 2.5° grade, 5° grade, 7.5° grade and 10° grade vehicle dynamic forces and power were examined and the relation of force and velocity along with power and velocity are shown in the figure 12,13,14,15 and 16 respectively.

At a 0° grade, the forces and power requirements are dominated by aerodynamic drag at higher velocities, with the aerodynamic force increasing from 1.61 N at 10 km/h to 40.41 N at 50 km/h, and aerodynamic power increasing from 4.47 W at 10 km/h to 561.34 W at 50 km/h. The accelerating force and power are significant at lower velocities, with the accelerating force starting at 5.56 N and accelerating power at 3.86 W, both increasing linearly with velocity. The rolling resistance force remains constant at 3.65 N, with rolling resistance power increasing linearly from 10.78 W to 50.685 W. There is no contribution from gradient resistance force and power due to the flat grade.

At a 2.5° grade, the force and power requirements for an E-bike are influenced by both aerodynamic drag and gradient resistance, with aerodynamic effects dominating at higher velocities. The aerodynamic force ranges from 1.61 N at 10 km/h to 40.41 N at 50 km/h, and the aerodynamic power increases significantly from 4.47 W to 561.34 W over the same range. The accelerating force and power also grow with velocity, starting at 5.56 N and 3.86 W, respectively. The rolling resistance force remains constant at 3.65 N, with the power rising linearly from 10.78 W to 50.68 W. The gradient resistance force is constant at 26.64 N, contributing significantly to the overall resistance, with the gradient power increasing linearly from 74.01 W to 552.71 W as velocity rises.

At a 5° grade, the force and power requirements for an E-bike are significantly influenced by both aerodynamic drag and gradient resistance. The aerodynamic force ranges from 1.61 N at 10 km/h to 40.41 N at 50 km/h, while the aerodynamic power increases from 4.47 W to 561.34 W over the same velocity range. The accelerating force and power also rise with velocity, beginning at 5.56 N and 3.86 W, respectively. The rolling resistance force remains constant at 3.65 N, with the rolling resistance power increasing linearly from 10.78 W to 50.68 W. The gradient resistance force, at a constant 53.28 N, significantly adds to the total resistance, with the gradient power increasing linearly from 148.02 W to 1104.37 W as velocity rises. This steep grade results in higher power demands, particularly for maintaining higher speeds.

At a 7.5° grade, the force and power requirements for an E-bike show substantial increases due to the combined effects of aerodynamic drag and gradient resistance. The aerodynamic force ranges from 1.61 N at 10 km/h to 40.41 N at 50 km/h, and the corresponding aerodynamic power increases from 4.47 W to 561.34 W. The accelerating force starts at 5.56 N, with accelerating power beginning at 3.86 W and rising quadratically with speed. The rolling resistance force is constant at 3.65 N, with the rolling resistance power increasing linearly from 10.78 W to 50.68 W as speed increases. The gradient resistance force, significant at a constant 79.63 N, dominates the total force, and the gradient resistance power rises linearly from 221.2 W to 1653.93 W as velocity increases. This steep gradient results in very high-power demands, especially at higher speeds, making it a challenging condition for the E-bike to maintain.

At a 10° grade, the force and power requirements for an E-bike are notably demanding, primarily due to increased aerodynamic drag and significant gradient resistance. The aerodynamic force varies from 1.61 N at 10 km/h to 40.41 N at 50 km/h, with corresponding aerodynamic power escalating sharply from 4.47 W to 561.34 W. The accelerating force starts at 5.56 N, and its power requirement begins at 3.86 W, increasing quadratically with velocity. Rolling resistance force remains constant at 3.88 N, while the rolling resistance power linearly increases from 10.78 W to 50.68 W. Gradient resistance force, which remains high at a constant 158.42 N, significantly contributes to the total force, and its power rises linearly from 296.04 W to 2200.34 W as velocity increases. Negotiating a 10° grade demands substantial power output, particularly at higher speeds, posing considerable challenges for the E-bike's performance.

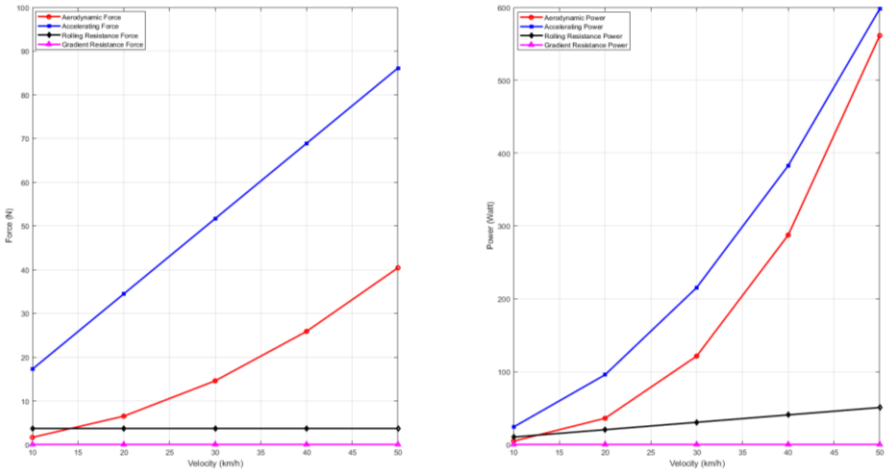

Figure 12. Relation of Force and Velocity (Left) and Power and velocity (Right) at Zero grade

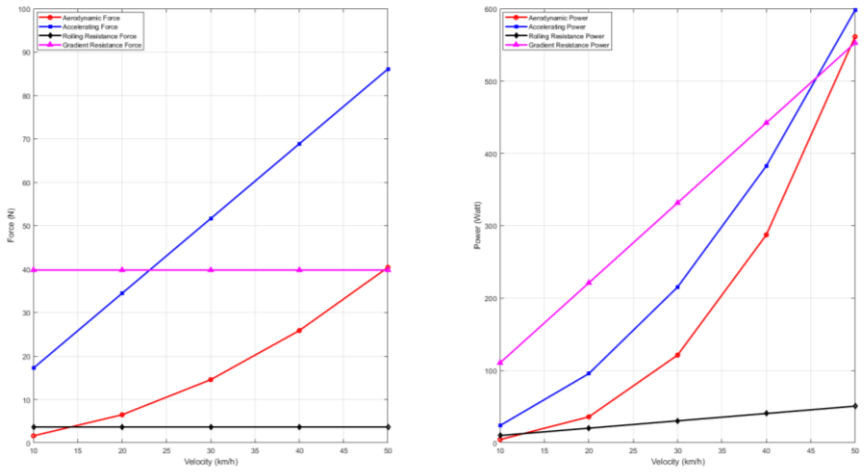

Figure 13. Relation of Force and Velocity (Left) and Power and velocity (Right) at 2.5 grade

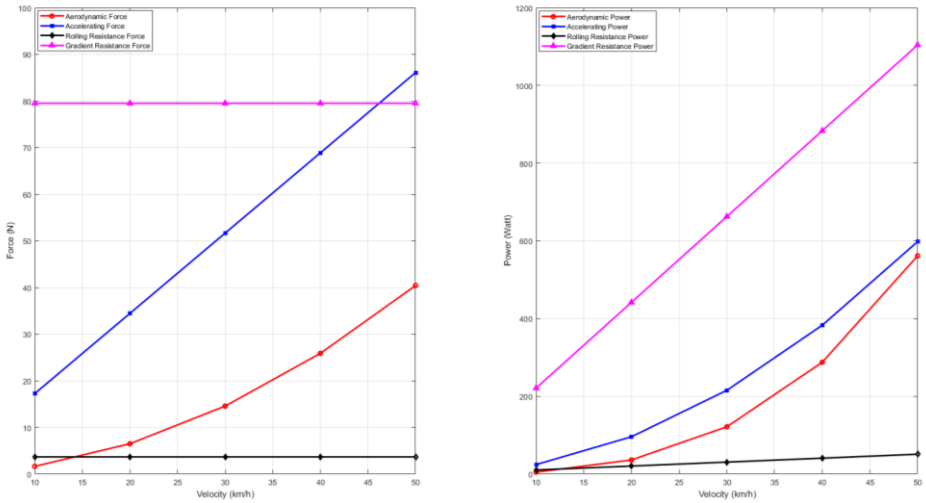

Figure 14. Relation of Force and Velocity (Left) and Power and velocity (Right) at 5 grade

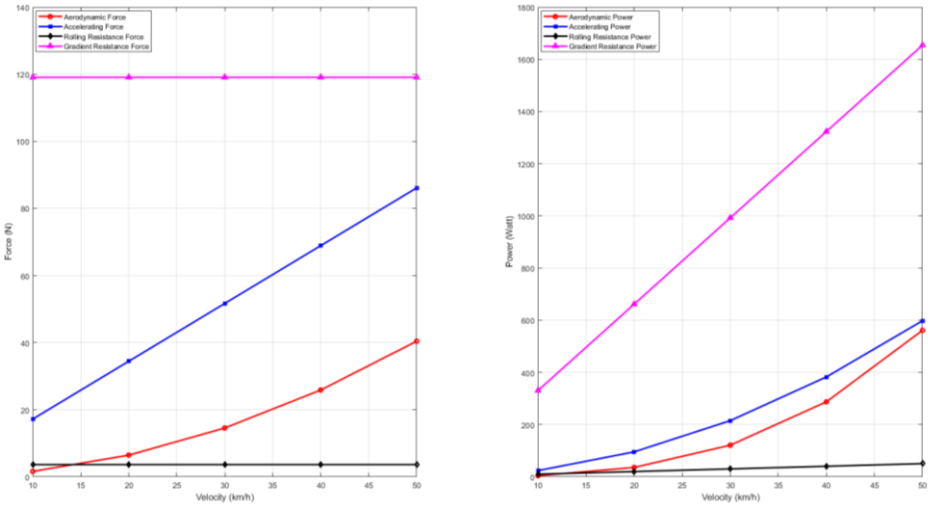

Figure 15. Relation of Force and Velocity (Left) and Power and velocity (Right) at 7.5 grade

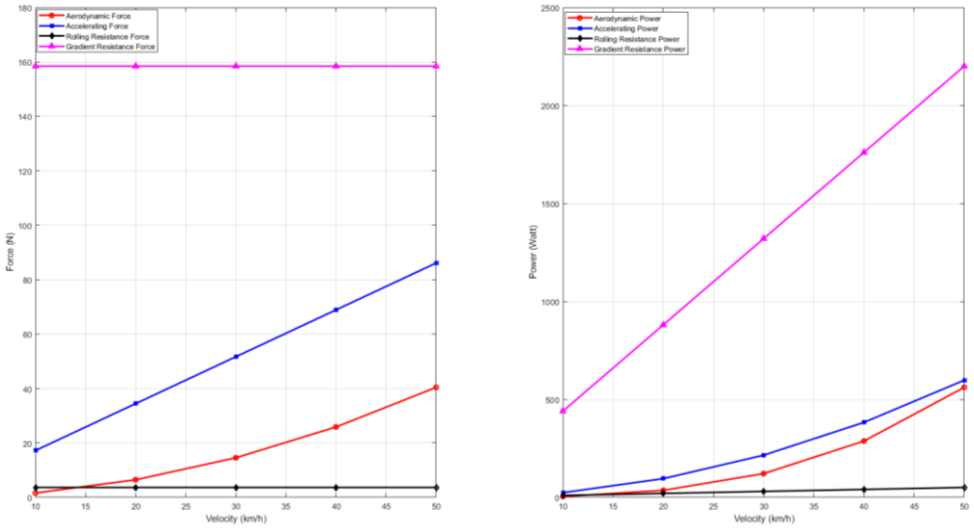

Figure 16. Relation of Force and Velocity (Left) and Power and velocity (Right) at 10 grade

5. Limitations and area of further research

A limitation of this study is that the regenerative braking and pedal charging systems were tested primarily in controlled environments, which may not fully capture the complexities and variability of real-world conditions such as diverse terrains, rider behaviors, and external factors like wind resistance or temperature fluctuations. Therefore, further real-world evaluation is needed to assess the practical effectiveness of these energy recovery systems and their overall impact on electric bicycle performance and energy efficiency. There is great section for further exploration and research such enthusiast can perform real-world practice and can advance the way of maximizing the regenerative braking and pedal charging systems.

6. Conclusion

This research demonstrated the potential of regenerative braking and pedal charging to enhance the energy efficiency of electric bicycles. The implemented regenerative braking system effectively captured braking energy, achieving a noteworthy 30.9% efficiency, which suggests a significant increase in range compared to traditional electric bicycles. While pedal charging exhibited a lower efficiency of 2.98%, it successfully generated electricity through rider pedaling, contributing to battery charge. This research addressed a gap in existing knowledge by focusing on these alternative methods, as prior studies likely concentrated primarily on battery capacity and motor efficiency. However, limitations exist, such as the controlled testing environment, which necessitates further real-world testing to understand the impact of varying conditions. MATLAB simulation data revealed distinctive trends in force and power requirements across different grades (0°, 2.5°, 5°, 7.5°, and 10°). At lower grades, aerodynamic forces and power requirements increased gradually with velocity, while accelerating forces and power requirements rose more steeply but remained moderate, with rolling and gradient resistance forces showing incremental yet manageable increases. As the grade steepened, aerodynamic forces and power requirements escalated sharply due to increased air resistance, dominating at higher velocities, while accelerating forces and power requirements rose quadratically with velocity and gradient resistance forces and power requirements increased linearly, significantly impacting overall power demand. These observations underscore the critical role of aerodynamic drag and gradient resistance in shaping performance and energy efficiency across varying terrain gradients. However, limitations such as the controlled testing environment necessitate further real-world testing to understand the impact of varying conditions. Overall, the findings highlight the promising potential of regenerative braking and pedal charging for improving electric bicycle efficiency. Overall, these findings highlight the promising potential of regenerative braking and pedal charging for improving electric bicycle efficiency. By building upon this research through further development and exploration of alternative energy capture and storage solutions, the future of electric bicycles holds great promise for sustainable and environmentally responsible transportation. (Giri et al., 2020)

References

Bansal, R., Sharma, A., Ali, M., Shrivastav, P., Yadav, V., Mandloi, S. and Dhanotia, R., 2020. DESIGN AND FABRICATION OF ELECTRIC BICYCLE. Advances and Applications in Mathematical Sciences,

Bigazzi, A. and Wong, K., 2020. Electric bicycle mode substitution for driving, public transit, conventional cycling, and walking. Transportation Research Part D: Transport and Environment, 85. https://doi.org/10.1016/j.trd.2020.102412.

Bucher, D., Buffat, R., Froemelt, A. and Raubal, M., 2019. Energy and greenhouse gas emission reduction potentials resulting from different commuter electric bicycle adoption scenarios in Switzerland. Renewable and Sustainable Energy Reviews, 114. https://doi.org/10.1016/j.rser.2019.109298.

Cabuk, A.S., 2022. Multiple Output Battery Charging Circuit for Bikers. Tehnicki Vjesnik, 29(2), pp.590–599. https://doi.org/10.17559/TV-20210414103953.

Chakraborty, S., Vu, H.N., Hasan, M.M., Tran, D.D., El Baghdadi, M. and Hegazy, O., 2019. DC-DC converter topologies for electric vehicles, plug-in hybrid electric vehicles and fast charging stations: State of the art and future trends. Energies, 12(8). https://doi.org/10.3390/en12081569.

Cherry, C.R., Weinert, J.X. and Xinmiao, Y., 2009. Comparative environmental impacts of electric bikes in China. Transportation Research Part D: Transport and Environment, 14(5), pp.281–290. https://doi.org/10.1016/j.trd.2008.11.003.

Dimitrov, V., 2018. Overview of the Ways to Design an Electric Bicycle. 9th National Conference with International Participation, ELECTRONICA 2018 - Proceedings. https://doi.org/10.1109/ELECTRONICA.2018.8439456.

Emadi, A., Lee, Y.J. and Rajashekara, K., 2008. Power electronics and motor drives in electric, hybrid electric, and plug-in hybrid electric vehicles. IEEE Transactions on Industrial Electronics, https://doi.org/10.1109/TIE.2008.922768.

Fishman, E. and Cherry, C., 2016. E-bikes in the Mainstream: Reviewing a Decade of Research. Transport Reviews, 36(1), pp.72–91. https://doi.org/10.1080/01441647.2015.1069907.

Giri, A., Gaikar, D., Mhatre, S. and Chavan, P., 2020. Electric bike with mileage enhancement.

Johny, S., Kakkattil, S.S., Sunny, S., Sandeep, K.S. and Sankar, V., 2021. Design and fabrication of foldable electric bicycle. Materials Today: Proceedings, 46, pp.9646–9651. https://doi.org/10.1016/J.MATPR.2020.07.157.

Kontar, W., Ahn, S. and Hicks, A., 2022. Electric bicycles sharing: opportunities and environmental impacts. Environmental Research: Infrastructure and Sustainability, 2(3). https://doi.org/10.1088/2634-4505/ac7c8b.

Kumar Choudhary B, S.G., Jadoun, R. and Kumar Choudhary, S., 2014. Design and fabrication of dual chargeable bicycle. [online] 5(8). Available at: <www.iiste.org>.

Mohan, K.V., Paritosh, M. and Jadhav, D.B., 2021. Design and Fabrication of Hybrid Electric Bicycle. International Research Journal of Engineering and Technology. [online] Available at: <www.irjet.net>.

Muetze, A. and Tan, Y.C., 2007. Electric bicycles - A performance evaluation. IEEE Industry Applications Magazine, 13(4), pp.12–21. https://doi.org/10.1109/MIA.2007.4283505.

Pattanayak, S.K., Tirkey, M., Lakra, P., Ranjan, V., Ranjan Panda, S. and Ranjan Panda, M., 2017. Electric Bicycle. International Journal of Scientific Development and Research, [online] 2(4). Available at: <www.ijsdr.org>.

Pellitteri, F., Campagna, N., Castiglia, V., Damiano, A. and Miceli, R., 2020. Design, implementation and experimental results of an inductive power transfer system for electric bicycle wireless charging. IET Renewable Power Generation, 14(15), pp.2908–2915. https://doi.org/10.1049/iet-rpg.2020.0056.

Prathyusha, P., Joshna, K., Harshitha, K., Hazira, S., Poojitha Reddy, M. and Engineering, E., n.d. HYBRID E-BICYCLE. [online] International Research Journal of Modernization in Engineering Technology and Science www.irjmets.com @International Research Journal of Modernization in Engineering, Available at: <www.irjmets.com>.

Ramadhan, A. and Dinata, R., 2021. Development of electric bicycle and its impact on the environment. IOP Conference Series: Materials Science and Engineering, 1122(1), p.012054. https://doi.org/10.1088/1757-899x/1122/1/012054.

Salmeron-Manzano, E. and Manzano-Agugliaro, F., 2018. The electric bicycle: Worldwide research trends. Energies, https://doi.org/10.3390/en11071894.

Shashank, R., Akshay, V., Ramesh, S., Nithin, B.G., Ravi, K.S. and Krishna, S.A.M., 2021. Design and fabrication of solar powered bicycle. In: Journal of Physics: Conference Series. IOP Publishing Ltd. https://doi.org/10.1088/1742-6596/2070/1/012208.

Somchaiwong, N. and Ponglangka, W., 2006. Regenerative power control for electric bicycle. In: 2006 SICE-ICASE International Joint Conference. pp.4362–4365. https://doi.org/10.1109/SICE.2006.314654.

Sousa, D.M., Costa Branco, P.J. and Dente, J.A., 2007. Electric bicycle using batteries and supercapacitors. In: 2007 European Conference on Power Electronics and Applications, EPE. https://doi.org/10.1109/EPE.2007.4417425.

Wei, L., Xin, F., An, K. and Ye, Y., 2013. Comparison Study on Travel Characteristics between Two Kinds of Electric Bike. Procedia - Social and Behavioral Sciences, 96, pp.1603–1610. https://doi.org/10.1016/j.sbspro.2013.08.182.

Yang, S., Lu, Y. and Li, S., 2013. An overview on vehicle dynamics. International Journal of Dynamics and Control, 1(4), pp.385–395. https://doi.org/10.1007/s40435-013-0032-y.